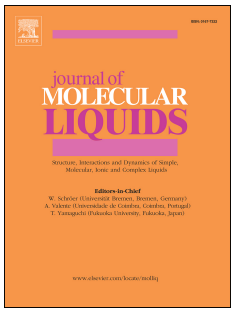

Molecular 5,8-π-extended quinoxaline derivatives as chromophores for photoluminescence applications

Leonardo de O. Aguiar, S.L. Adalberto, Ivan H. Bechtold, Sergio Fernando Curcio, Thiago Cazati, Tiago V. Alves, André Alexandre Vieira

PII: S0167-7322(19)33223-4

DOI: https://doi.org/10.1016/j.molliq.2019.111763

Reference: MOLLIQ 111763

To appear in: *Journal of Molecular Liquids*

Received Date: 7 June 2019

Revised Date: 23 July 2019

Accepted Date: 17 September 2019

Please cite this article as: L.d.O. Aguiar, S.L. Adalberto, I.H. Bechtold, S.F. Curcio, T. Cazati, T.V. Alves, André.Alexandre. Vieira, Molecular 5,8-π-extended quinoxaline derivatives as chromophores for photoluminescence applications, *Journal of Molecular Liquids* (2019), doi: https://doi.org/10.1016/j.molliq.2019.111763.

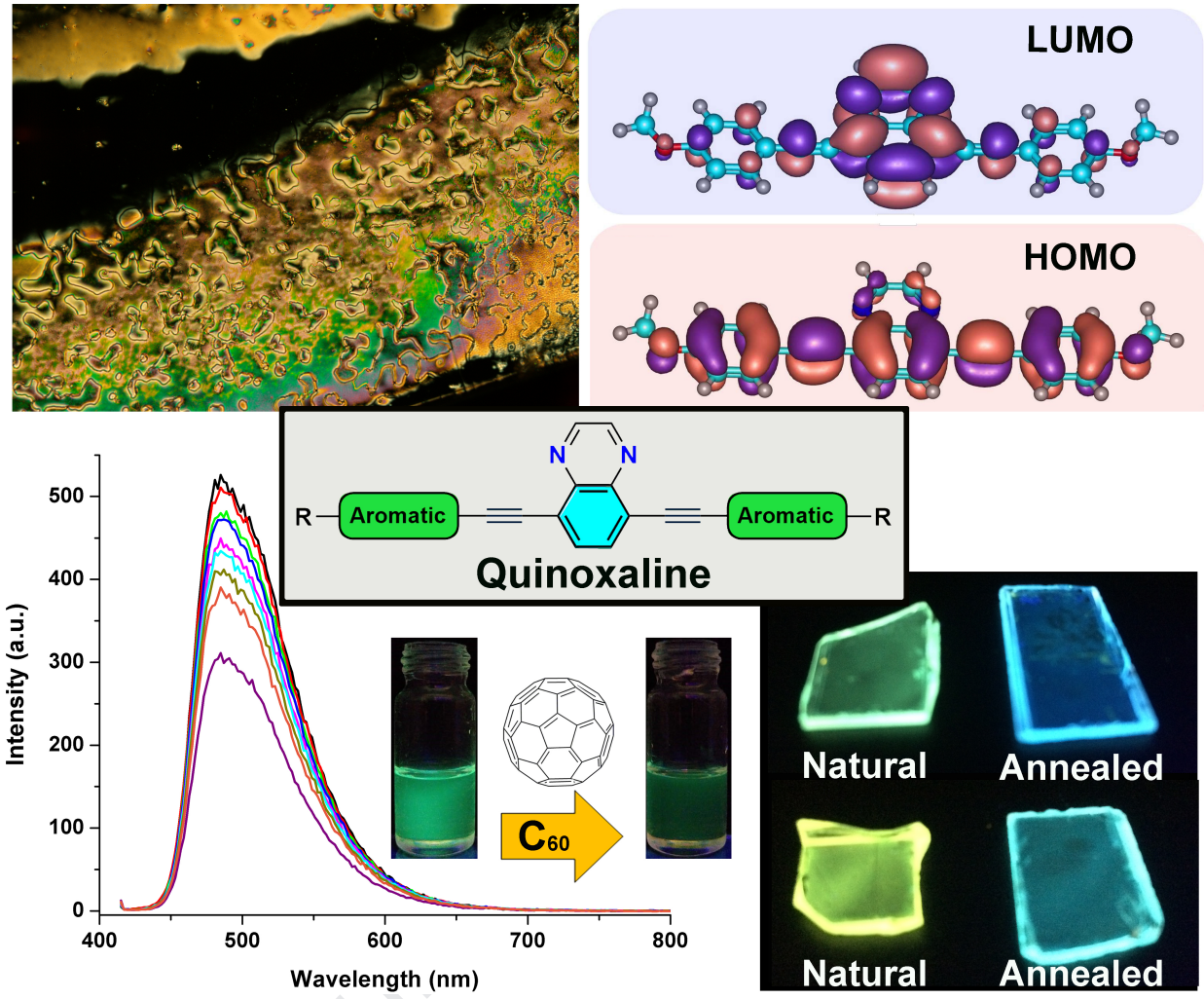

Molecular 5,8-π-Extended Quinoxaline Derivatives as Chromophores for Photoluminescence Applications

Leonardo de O. Aguiar[a], Adalberto S. L. Junior[a], Ivan H. Bechtold[b], Sergio Fernando Curcio[c], Thiago Cazati[c], Tiago V. Alves[a] and André Alexandre Vieira[a]

[a]Instituto de Química, Universidade Federal da Bahia, 40170-115. Salvador, Bahia, Brazil.

[b]Departamento de Física, Universidade Federal de Santa Catarina, 88040-900, Florianópolis, SC, Brazil.

[c]Departamento de Física, Universidade Federal de Ouro Preto, 35400-000 Ouro Preto, MG, Brazil.

Keywords: Quinoxaline, luminescence, liquid crystals, synthesis.

*email: Vieira.andre@ufba.br

Abstract

The 5,8-π-extended quinoxaline derivatives are widely studied due to their well-known photophysical and electrochemical properties. In order to investigate the structure-property relationship, a novel series of fluorescent calamitic liquid crystals based on the quinoxaline heterocycle was successfully synthesized and characterized. The final molecules presented calamitic mesomorphism with nematic and smectic phases. These compounds displayed intense green photoluminescence under UV light excitation in solution and in the solid state. In chloroform solution, the fluorescence quantum yields (Φ_{FL}= 0.54–0.62) of the quinoxaline-based derivatives were significantly higher than those previously described for similar benzothiadiazoles. The maximum emission peaks were between 511-520 nm with singlet excited-state lifetimes in the nanosecond timescale. The solvatochromism studies showed a significant dependence of the emission on the polarity of the solvent. Doping of the quinoxalines with fullerene C_{60} suggests a charge transfer process, this being dependent on the π-conjugate core. The energy band gaps predicted with DFT calculations are in excellent agreement with the experimental data.

Introduction

Organic fluorescent dyes with designed emission characteristics have become widely used [1-3] and the areas of application are varied, including in organic electronics[4], for instance, in organic field effect transistors (OFETs), organic light-emitting diodes (OLEDs) and dye-sensitized solar cells (DSSCs)[5, 6] and in bioanalytical imaging, sensing [7, 8], and diagnostics[9].

Luminescent liquid crystals (LLCs) have attracted considerable interest because of advantages such as supramolecular self-assembly, anisotropic fluid properties and intrinsic light-emitting ability.[10, 11] As a consequence, the demand for novel LLC molecules presents a challenge in the area of synthetic chemistry and, with regard to the photophysical properties, consistent structure–property correlations need to be established. Several LLCs are described in the literature, but the quinoxaline heterocycle has not been explored in the preparation of calamitic liquid crystals.

Quinoxaline, also called benzopyrazine, is a heterocyclic compound containing a ring complex made up of a benzene ring and a pyrazine ring[12, 13]. The quinoxalines are an important class of N-heterocycles, which have found numerous applications in biological studies,[14, 15] fluorescent dyes,[13, 16] and as a backbone for functional materials.[17, 18] In particular, 5,8-π-extended quinoxalines have been used as building blocks in photoluminescent and electroluminescent materials because they generally show high electron affinity and good thermal stability,[19, 20] and they can also act as electron-transporting materials.[21-23] These derivatives have been successfully incorporated into polymers and molecules for use as electron-transport materials in multilayer OLEDs.[24-28] Furthermore, quinoxaline derivatives

present the advantage that they can be easily modified by attaching various side chains, such as alkyl/alkoxy chains, aromatic rings and functional groups.

The synthesis of extended π-conjugated systems has been the key to providing LLCs. These compounds are often based on a push-pull system, comprised of an electron-donating group (D) and an electron withdrawing group (A) linked through a π-conjugated spacer. In a previous study, we systematically developed electrooptical liquid crystals based on a "D-π-A-π-D" architecture, which contains different heterocycles as the acceptor unit, for the design of more efficient organic systems with improved spectral response and photo/thermal properties.

Herein, we report the design, synthesis and characterization of a series of luminescent liquid crystals based on the 5,8-π-extended quinoxaline system. The mesomorphic and photophysical properties of the target molecules were investigated. Surprisingly, a high reactivity of the quinoxaline was verified via the Sonogashira reaction and pronounced relative quantum yields were obtained, in contrast to results previously reported in the literature [29].

Results and discussion

Synthesis

The synthetic route used to obtain the target molecules **5a-g** is shown **Scheme 1** and the same procedure was adopted in our previous research[30]. It starts from the sulfur extrusion reaction of 4,7-dibromo-2,1,3-benzothiadiazole (**1**) with sodium borohydride and catalytic cobalt chloride in a mixture of ethanol/tetrahydrofuran to obtain the diamine (**2**) in 75% yield. The 3,6-dibromobenzene-1,2-diamine was subjected to a condensation reaction with

glyoxal, triethylamine and ethanol at room temperature to afford the 5,8-dibromoquinoxaline (**3**) in 70% yield. The aryl acetylenes **4a-g** were synthetized from the respective aryl halides via palladium catalyzed cross-coupling using 2-methyl-3-butyn-2-ol, followed by protective group elimination. The compounds **5a-g**, with π-extended conjugation presenting the quinoxaline moiety, were obtained via the Sonogashira coupling reaction between one equiv. of the building block **3** and two equiv. of the corresponding aryl acetylene **4a-g**, using bis(triphenylphosphine)palladium (II) dichloride, triphenylphosphine, copper iodide dissolved in triethylamine and tetrahydrofuran solvents. After purification, the desired final molecules were obtained in good yields (55-84%). This synthetic strategy is appropriate since the quinoxaline **3** proved to be a very reactive nucleus for the Sonogashira cross coupling and the final reactions occurred, in general, within 20 min. This result was unexpected, because the literature describes 5,8-dibromoquinoxaline as a non-reactive system.[29]

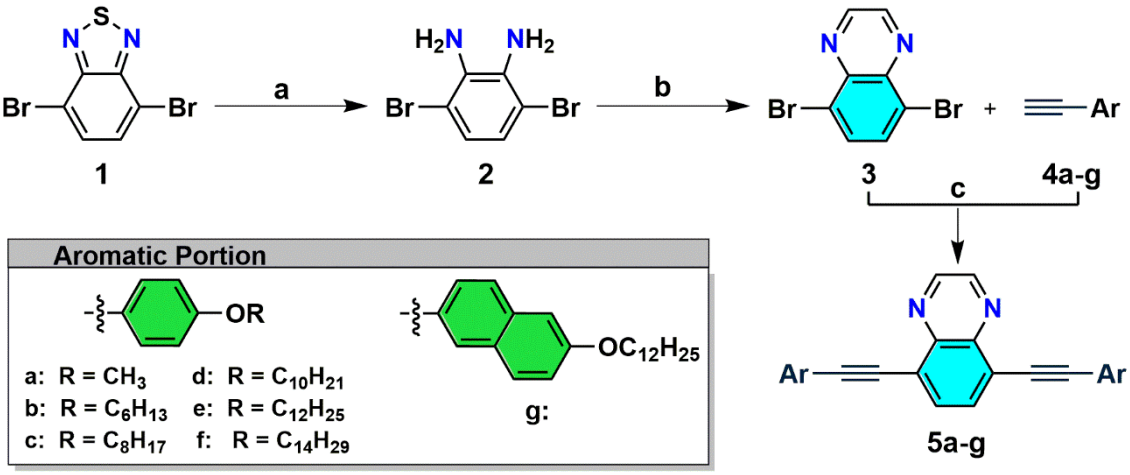

Reagents and Conditions: (**a**) $NaBH_4$, $CoCl_2$. $6H_2O$, THF/EtOH; (**b**) Glyoxal, EtOH, NEt_3; (**c**) $PdCl_2(PPh_3)_2$, CuI, TPP, NEt_3/THF.

Scheme 1. Synthesis of the target compounds **5a-g**.

All of the final molecules synthesized (**5a-g**) were characterized by spectroscopic methods and APPI mass spectrometry.

Liquid crystalline behavior

The thermal properties of compounds **5a-g** were studied by differential scanning calorimetry (DSC) and polarized optical microscopy (POM). The transition temperatures and enthalpy values are summarized in **Table 1**. The liquid crystalline properties of the final compounds were confirmed by X-ray diffraction (XRD).

Table 1. Phase transition temperatures (℃) and enthalpies ($kJ \cdot mol^{-1}$) for compounds **5a-g.**

Compound	Transition [c]	T/℃, heating ($\Delta H/kJ.mol^{-1}$) [a]	T/℃, cooling ($\Delta H/kJ.mol^{-1}$) [a]	$T_{dec.}$/℃ [b]
5a	Cr-Iso	161	107	322
5b	Cr-N N-Iso	154 (18.2) 172 (0.3)	133 (23.1) 167 (0.1)	388
5c	Cr-N N-Iso	146 (21.2) 167 (2.0)	132 (21.8) 166 (2.7)	409
5d	Cr(I)-Cr(II) Cr(II)-SmC SmC-N N-Iso	118 (4.5) 138 (24.6) 160 (7.0) 165 (broad)	117 (4.4) 130 (24.6) 159 (4.7) 162 (broad)	347
5e	Cr(I)-Cr(II) Cr(II)-Cr(III) Cr(III)-SmC SmC-Iso	54 (9.5) 124 (5.6) 129 (12) 159 (3.0)	40 (5.5) --- 119 (12.2) 156 (0.7)	396
5f	Cr(I)-Cr(II) Cr(II)-SmC SmC-Iso	68 (9.2) 124 (26.8) 159 (4.9)	63 (9.9) 115 (26.5) 158 (4.1)	354
5g	Cr-SmC SmC-Iso	160 (30.3) 231 (3.3)	138 (12.8) 225 (1.0)	301

[a]Determined by POM and DSC measurements (10 ºC/min) on the second heating cycle. [b]Determined by TGA, onset of decomposition in nitrogen (10 ºC/min). [c]Cr = Crystal, N = Nematic, SmC = Smectic C, I = Isotropic liquid.

All the final compounds, with the exception of **5a**, exhibited liquid crystalline behavior, with nematic and smectic phases being present, which are typical of calamitic-like molecules. The elongation of the aromatic moieties linked to the 5,8-quinoxaline and the alkoxy chain lengths allow a broader mesomorphic range and the appearance of more organized phases, such as the smectic phase. This behavior can be attributed to an increase in the length-to-breadth ratio of the molecule.

The mesophases were identified according to the classification reported by Dierking and Demus.[31] The cooling of the samples **5b**, **5c** and **5d** from the isotropic phase showed birefringent liquid droplets, which later agglutinate to give the schlieren texture typical of a nematic mesophase. During the slow cooling of the nematic phases, a strong tendency to exhibit homeotropic behavior was observed. **Figure 1a** shows the fully homeotropic alignment of compound **5c** at 150 ℃ and **Figure 1b** shows **5d** at 161 ºC at the beginning of the alignment process. By further cooling of **5d**, the nematic phase transitions to a SmC phase, leading to the characteristic broken fan-shaped texture. The SmC phases were confirmed also on cooling samples **5e-g** from the isotropic state, with the growth of smectic batonnets. Selected imagens of the SmC mesophases for **5e** and **5f** are shown in **Figure 1**.

The DSC analysis confirmed the liquid crystalline transitions observed by POM in both the heating and cooling cycles. The mesomorphism found was shown to be dependent on the length of the alkoxy chains attached to the center and the aromatic π-extended moiety. Compound **5a** did not show a mesophase, which was expected due to the absence of the long alkyl chains. Molecules **5b** and **5c** of the series exhibit only the nematic phase during heating

and cooling. A variation in the length of the alkoxy chains did not change the type of mesomorphism or range presented, but there was a decrease in the melting point, the crystal-to-nematic transition being observed at 154 ºC and 146 ºC for **5b** and **5c**, respectively. The increase in the length of the alkoxy group to C10 (**5d**) led to a suppression of the nematic phase (ΔT_N = 3) and favored the smectic C (ΔT_{SmC} = 29) phase.

The compounds with longer alkoxy chains (**5e** and **5f)** presented exclusively the formation of smectogenic phases and the highest mesomorphism range of this homologous series (ΔT_{SmC} = 37 and ΔT_{SmC} = 43, respectively). The exchange of the phenyl group with naphthyl in **5g** raises the melting temperature of quinoxaline, but also gives higher stability to the SmC phase (ΔT_{SmC} = 87). These results show the influence of the alkoxy chain length on the occurrence of calamitic mesomorphism.

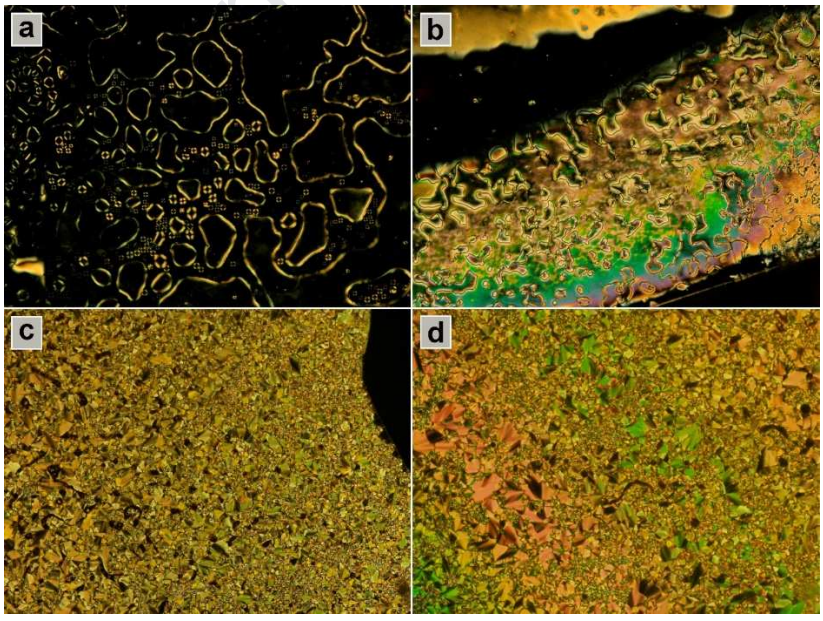

Figure 1. Polarized optical photomicrographs of compounds (a) **5c** at 150 ºC (100x), (b) **5d** at 161 ºC (100x), (c) **5e** at 140ºC (100x) and (d) **5f** at 176ºC(200x) in the cooling cycle.

High thermal stability of the final molecules was determined by thermogravimetric analysis (TGA), with decomposition temperatures above 300℃. The naphthyl derivative **5g** had the lowest decomposition temperature (T_{dec} = 301 ℃), while the phenylene derivatives **5a-f** exhibited higher stability (T_{dec} = 322-409 ℃).

X-ray diffraction studies

X-ray diffraction experiments were carried out to confirm the structure of the SmC phases observed by POM for compounds **5d, 5e** and **5f**. All spectra showed an intense peak in the low-angle region (d_{001}), which is associated with the interlayer spacing, and secondary peaks, where the ratio with d_{001} gives integers, confirming the lamellar character of the smectic mesophase.[32] A diffuse peak was observed at around $2\theta = 20^{o}$, which corresponds to a distance of 4.5 Å. This represents the lateral distance between the neighboring molecules within the layers.[33] On comparing the first diffraction peak d_{001} with the molecular length L (estimated by ChemBio3D Ultra software, version 11.0.1), one can infer that the aliphatic chains are folded or the molecules are tilted within the layers (or both). Considering the molecules in the most extended form (although this is not usually the case) the tilt angle (θ) of the SmC phase was estimated using the relationship $\cos\theta = d_{100}/L$, see values in **Table 2**. The results indicate that the tilt angle increases for longer aliphatic chains and, if this is not the case, the longer chains must be more folded. **Figure 2** shows a representative spectrum (for compound **5d)**.

Table 2. Structural parameters of compounds **5d, 5e** and **5f** in the SmC phase.

Compound	L (Å)	d_{001} SmC (Å)	Tilt angle θ (°)
5d	43.1	36.2	33
5e	48.1	37.5	39
5f	53.2	38.7	43

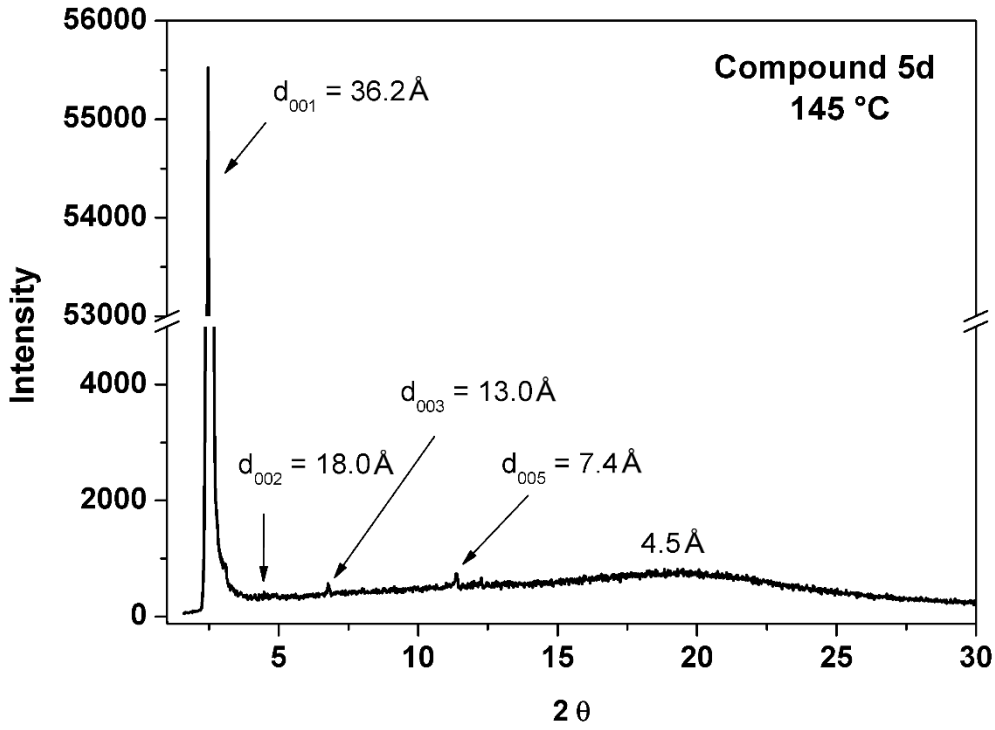

Figure 2. X-ray pattern for compound **5d** collected at 145 ºC in the SmC mesophase.

Photophysical properties

UV-vis and Fluorescence

The ultraviolet−visible absorption and fluorescence spectra for the quinoxaline derivatives **5a-g** were collected using a dilute solution (M = 1.0 × 10^{-5} mol/L) in chloroform, and in thin films prepared by spin coating onto quartz substrates (**Figure 3** and **5)**. The chloroform solvent was chosen because of the high solubility of the molecules therein. Relevant data are summarized in **Tables 3** and **4**.

Table 3. Photophysical properties of **5a–g** in chloroform solution.

Sample	Absorption[b] λ_{max} (nm) (ε/ 10^4 M^{-1} cm^{-1})[a]	Emission λ_{max} (nm)[b,c]	Stokes Shift (nm)	Φ_f [d]	τ_f / ns	τ_0 [e] / ns	k_r [f] (s^{-1}) ($x10^8$)	K_{nr} [f] (s^{-1}) ($x10^8$)
5a	409 (2.8)	518	109	0.62	5.76	9.29	1.08	0.66
5b	409 (2.4)	518	109	0.59	5.62	9.53	1.05	0.73
5c	410 (3.5)	520	110	0.59	5.60	9.49	1.05	0.73
5d	411 (4.0)	518	107	0.62	5.61	9.05	1.11	0.68
5e	410 (4.9)	520	110	0.55	5.59	10.16	0.98	0.81
5f	411 (2.1)	518	107	0.56	5.59	9.98	1.00	0.79
5g	419 (2.0)	511	92	0.54	4.05	7.50	1.33	1.14

[a]Units = L $mol^{-1}cm^{-1}$; [b]chloroform solution (1.0 x 10^{-5} mol L^{-1}); [c]excited at maximum absorption; [d]relative quantum yields in solution determined using quinine sulfate as standard (Φ_{FI} = 0.546 in 1N H_2SO_4). [e]Natural radiative lifetime calculated using $\tau_0=\tau_f/\Phi_f$. [f]k_r and k_{nr} are the radiative and non-radiative rate constants calculated using $k_r = \Phi_f / \tau_f$ and $k_{nr} = (1-\Phi_f) / \tau_f$, respectively.

Compounds **5a-f** exhibited strong absorption bands in the ultraviolet region, with maxima at around 410 nm, and molar extinction coefficients in the range of 20,000−49,000 L.$mol^{-1}cm^{-1}$. These absorption bands are assigned to π–π* transitions. The position of the absorption maxima was not significantly altered with different lengths of the alkoxy chains (**5a-f**). The highest absorption peak for **5g** was red-shifted by 9 nm compared with the average. This could be due to an electronic effect, which lowers the HOMO-LUMO band gap due to the presence of an elongated conjugation by the naphthyl group.[34] All of the final compounds exhibited a similar and intense yellowish green luminescence when excited at the maximum absorption wavelength in chloroform solution (λ_{exc} = 410 nm). The maximum emission peaks were observed between 450 and 600 nm (**Figure 3**). The fluorescence spectra for **5a-f** are similar and showed emission maxima at 518-520 nm. The naphthyl derivative **5g** presented a slight blue-shift with emission maxima at 511 nm. The observed Stokes shifts were in the range of 92–110 nm, with a small region of coincidence between the absorption and emission wavelengths. All molecules **5a-g** exhibited good quantum yields in chloroform solution (Φ_f = 0.54-0.62), and these were

significantly higher than those for similar benzothiadiazoles (Φ_f = 0.19-0.20)[35]. This difference can be attributed to the nitrogen atoms in the quinoxaline π-conjugate system, which does not suffer from the heavy atom effect[30, 36, 37]. The quantum yields are higher than those reported by Mancilha[29], probably due to the influence of the triple bonds in compounds **5a-g**, which increase the π-conjugation length of the system[38-40].

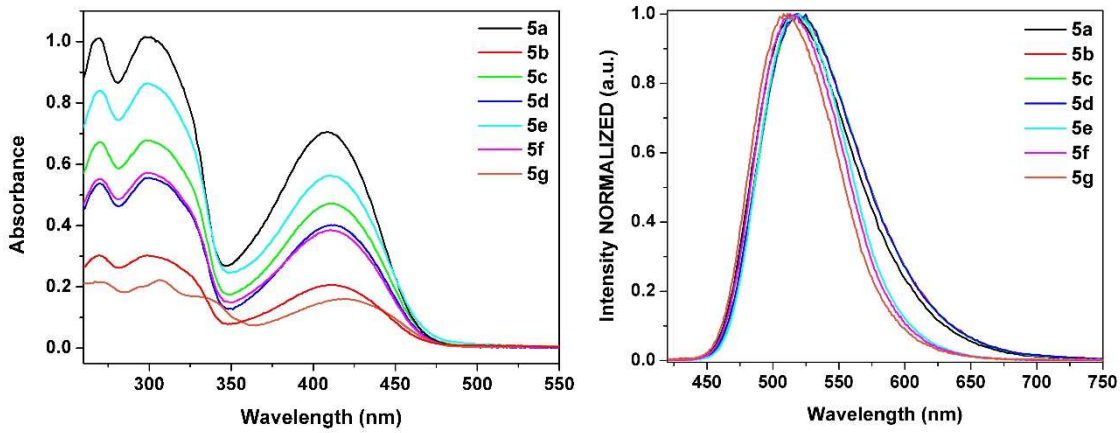

Figure 3. Absorbance (left) and emission (right) spectra of the compounds **5a-g** in chloroform solution (10^{-5} mol/L).

The singlet excited-state lifetimes for compounds **5a-g** in chloroform solution were measured at the maxima of the emission intensity after excitation at 401 nm by time-resolved fluorescence spectroscopy and their fluorescence decay curves can be seen in the supporting information. All compounds exhibited mono-exponential fluorescence decay with lifetimes in the nanosecond timescale, characteristic of monomeric emission, see values in **Table 3**. The singlet excited-state lifetimes (τ_f) of compounds **5a-f** were similar, suggesting that the lifetimes are not significantly affected by the alkoxy chain length. Compound **5g**, with a conjugation elongated by the naphthyl group, showed the shortest lifetime. The values

obtained are similar to the lifetimes reported for other benzoheteroarene–ethynylene systems.[41]

The natural radiative lifetimes (τ_0) and radiative (k_r) and non-radiative (k_{nr}) fluorescence constants are also shown in **Table 3.** Considering $\tau_0=\tau_f/\Phi_f$, $k_r=\Phi_f/\tau_f$ and $k_{nr}=(1-\Phi_f)/\tau_f$.

Thin films of compounds **5b-g** were investigated before and after annealing, consisting of heating the film until it melted, followed by cooling at 10ºC/min. Compound **5a** did not form a homogeneous film, probably due to the absence of alkyl chains. Interestingly, before annealing the **5b-g** films exhibited hypsochromic shifts of around 40 nm and 34 nm for the absorption and emission bands, respectively, in relation to the solution.

Table 4. Summary of photophysical properties of **5b–g** obtained in thin film analysis.

Sample	Absorption λ_{max} (nm) Natural	Absorption λ_{max} (nm) Annealed	Emission λ_{max} (nm)[a] Natural	Emission λ_{max} (nm)[a] Annealed	E_{gap}^{op} (eV)[b]
5b	364	345	463	458	2.84
5c	365	356	484	459	2.89
5d	366	358	494	455	2.90
5e	368	359	485	459	2.86
5f	368	360	498	458	2.88
5g	421	354	517	478	2.79

[a]Excited at maximum absorption; [b]Optical bandgap calculated on the low energy edge of the absorption spectrum (E_{gap}^{op} = 1240/λ_{onset}).

After the annealing of the films, **5b-g** showed hypsochromic shifts in the absorbance and emission spectra in the range of 11 nm and 27 nm, respectively.

This is probably related to H-aggregate formation in the quinoxaline films[42]. An H-aggregate is a one-dimensional array of molecules in which the transition dipole moments of individual monomers are aligned parallel to each other but perpendicular to the line joining their centers (face-to-face fashion), thereby increasing the energy transition and shifting the absorption band to shorter wavelengths, according to Kasha's exciton model[43, 44]. The emission spectra for compounds **5d** and **5g** obtained before and after annealing are shown in **Figure 4**. The emission displacement is evidenced from the change in the photoluminescence color.

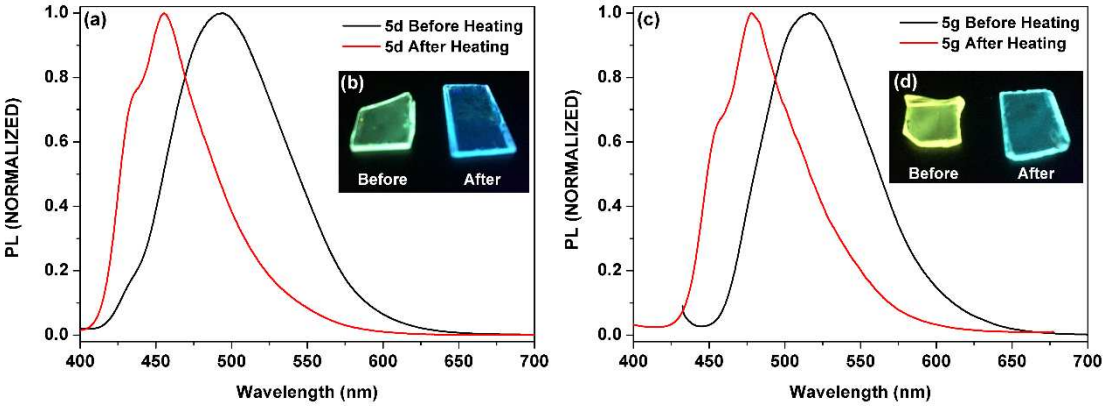

Figure 4. Emission spectra for thin films of **5d (a)** and **5g (c)** before and after annealing, **(b)** and **(d)** show illustrative photographs of the films.

Solvatofluorochromism properties

Compounds **5b** and **5f** were chosen to investigate the solvatofluorochromism of the quinoxaline derivatives. The optical properties were measured in commonly used organic solvents such as heptane, acetone, acetonitrile, chloroform, dimethylformamide, tetrahydrofuran and toluene. The results indicate a significant dependence of the emission characteristics on the solvent polarity,

which had only a slight effect on the absorbance spectra. **Figure 5** shows the emission and absorbance spectra for **5b** in the different solvents (all of the data are summarized in the Electronic Supporting Information).

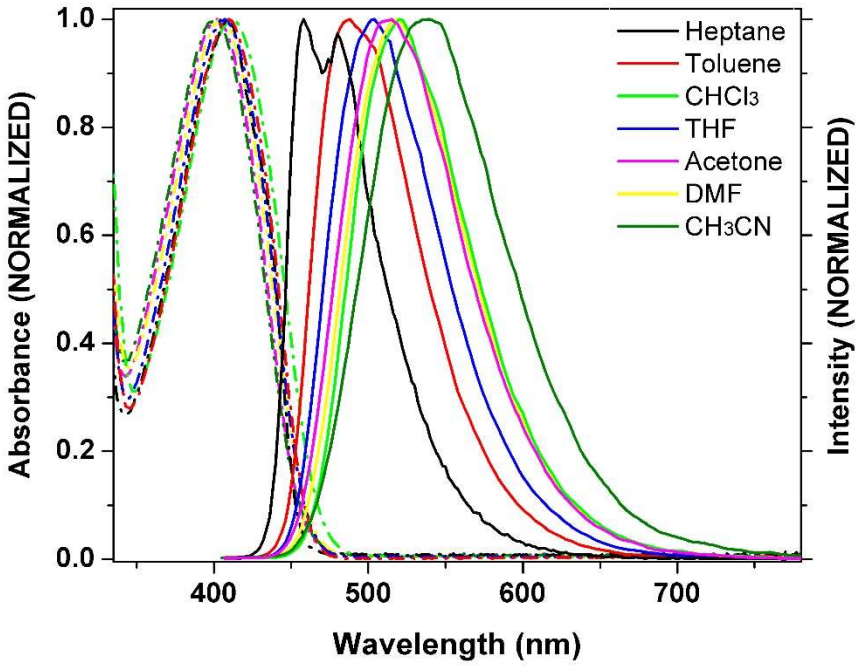

Figure 5. Normalized absorbance (dashed line) and emission (solid line) spectra for **5b** in different solvents.

The compounds **5b** and **5f** have well-resolved absorption and emission bands. The maximum emission bands are shifted to longer wavelengths by increasing the solvent polarity, e.g., from 458 nm (hexane) to 537 nm (acetonitrile) in the case of **5b**. This represents a variation of 79 nm in the luminescence of the quinoxaline derivatives. The length of the alkoxy chains has no influence on the solvatofluorochromism of **5b** and **5f** in the solvents studied.

The solvent-sensitivity of the fluorophore was estimated using the Lippert-Mataga equation.[45, 46] The plot of the Stokes shifts (Δv) as a function of

orientation polarizability (Δf) for **5b** is shown in **Figure 6**. The increase in Δv with an increase in the solvent polarity parameter leads to a linear correlation of 0.906 for **5b** and 0.902 for **5f** (see Electronic Supporting Information).

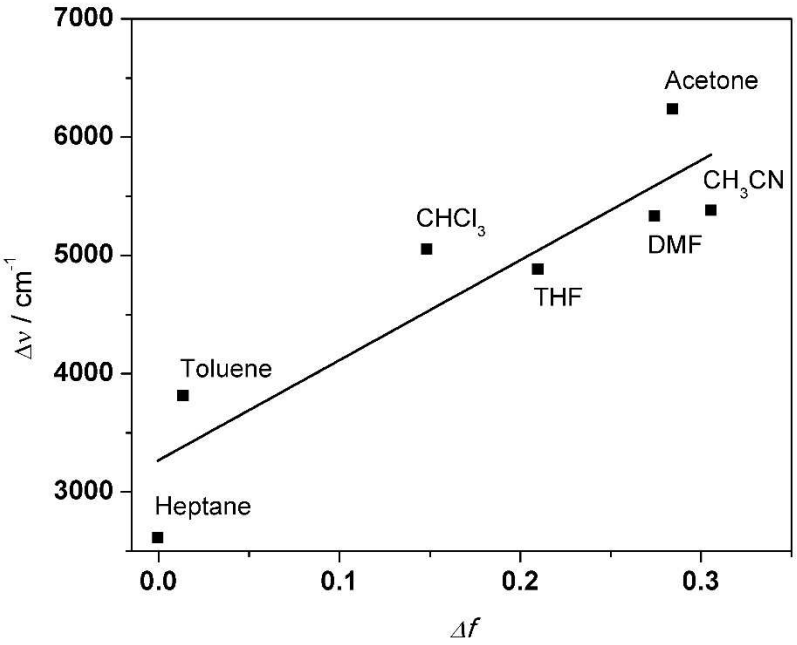

Figure 6. Changes in the Stokes shifts (Δv) for **5b** versus Δf for the different solvents.

Slopes of 8457 and 8344 were obtained for **5b** and **5f**, respectively. This indicates that the dipole moment of quinoxalines in the excited state is higher than in the ground state. In addition, the similarity of the slopes of the Lippert-Mataga plots for **5b** and **5f** suggests that the alkoxy chains have no effective influence on the solvatochromism of these architectures.

Molecular orbital calculations

In order to obtain further evidence of the optical properties of the molecules investigated, we performed quantum chemical calculations with density functional theory (DFT) using the Gaussian 09 software. In this step, the calculations were carried out for two different compounds obtained experimentally, **5a** and **5g**. To reduce the computational time, we replaced the $–OC_{12}H_{25}$ group with $–OCH_3$ in the structure of **5g** (referred to as **5g***). The geometry optimizations were calculated using the Becke three-parameter set with the Lee-Yang-Parr modification (B3LYP) together with the 6-31+G(d,p) basis set. The vibrational harmonic frequencies were determined to confirm the nature of the stationary points on the potential energy surface. The cartesian coordinates of the optimized structure and the 3N-6 harmonic vibrational frequencies are listed in **Tables S.I and S.II** in the Supporting Information. **Figure 7** shows the optimized geometries and the molecular amplitude plots of the HOMO and LUMO energy levels with a molecular orbital for **5a** and **5g***. The LUMO distribution of these compounds is mainly on the quinoxaline core, while the electron density of the HOMO is mainly distributed between the substituted phenyl/naphthyl and quinoxaline groups, indicating an electronic conjugation between them. Although the HOMO energy levels of **5a** and **5g*** are identical (–5.40 eV), a higher electron density dispersion is observed for the naphthyl derivative, promoting a greater electronic conjugation of compound **5g*** compared to **5a**. Moreover, at the B3LY/6-31+G(d,p) level of theory, the energy band gaps for **5a** and **5g*** are 2.85 and 2.78 eV, respectively. The theoretical energy gap for **5g*** (2.78 eV) is in excellent agreement with the value obtained experimentally in the thin film analysis (2.79 eV).

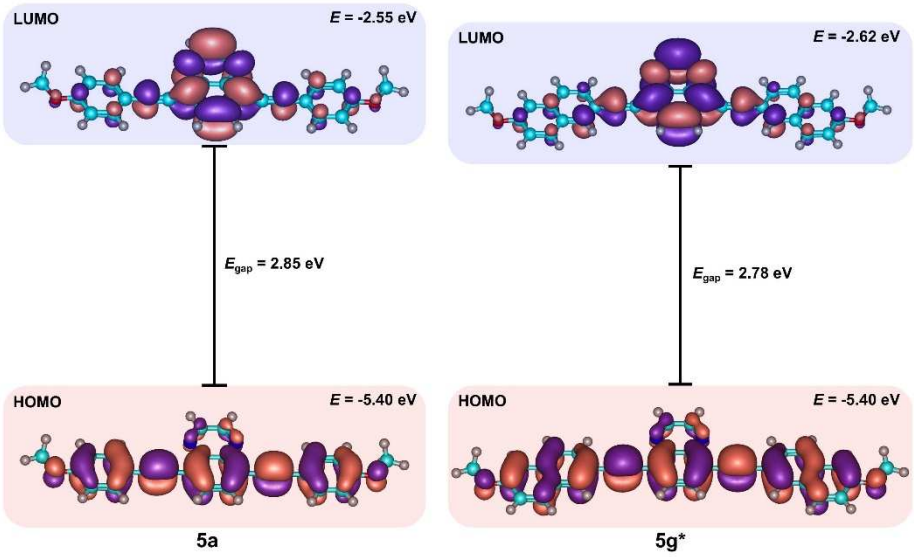

Figure 7. Optimized structures, molecular orbital diagrams for the HOMO and LUMO, and band gap energies for **5a** and **5g***, obtained at the DFT/B3LYP/6-31+G level of theory.

Preliminary photoinduced charge separation

To investigate the possibility of the charge transfer process, fluorescence quenching experiments were carried out with the quinoxalines **5e** and **5g** (**Figure 8)**. The fluorescence of the quinoxalines in toluene solution was gradually quenched by doping with fullerene C_{60}.

This behavior suggests a photoinduced charge separation process involving quinoxaline as the donor and fullerene as the acceptor.[47, 48] Moreover, the dependence of the fluorescence intensity on the C_{60} concentration is linear, in accordance with the Sterne-Volmer equation:

$$F_0/F = 1 + K_{sv}[C]$$

where F_0 and F represent the fluorescence intensity in the absence and presence of C_{60}, respectively, K_{sv} is the quenching constant and [C] is the

concentration of C_{60}. Thus, the *Ksv* values for **5e** and **5g** are 4.66 x 10^3 M^{-1} and 5.84 x 10^3 M^{-1}, respectively. This suggests charge transfer between the quinoxaline and C_{60} [49]. In addition, the difference in the *C* values for **5a** and **5g** indicates that the larger core may have a greater electron transfer capacity.

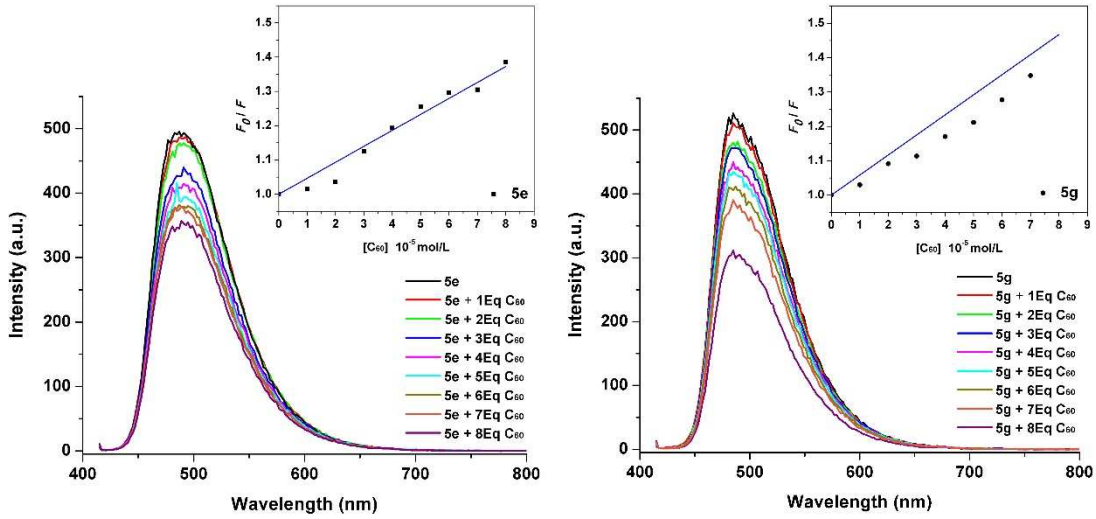

Figure 8. (a) Emission spectra for **5e** and **5g** (1.8 × 10^{-5} M) in toluene with increasing concentration of C_{60}: 0.0 (blank), 1.0 equiv. (1), 2.0 equiv. (2), 3.0 equiv. (3), 4.0 equiv. (4), 5.0 equiv. (5), 6.0 equiv. (6), 7.0 equiv. (7), 8.0 equiv. (8). The insets show the Sterne-Volmer quenching plots for these compounds.

Conclusions

In summary, a series of luminescent liquid crystal derivatives obtained with the 5,8-bis(phenylethynyl)quinoxaline core was successfully synthesized and characterized. The relationship between the mesomorphism and the length-to-width ratio was explored through compounds with different alkoxy chains. The final compounds showed predominantly nematic and smectic mesophases. An increase in the length of the alkoxy chain suppressed the nematic phase and favored the smectic phase. These molecules exhibited strong green fluorescence with maxima between 450 and 600 nm and pronounced quantum yields in solution (0.54 to 0.62), values much higher than materials without the

ethynylene spacer. All compounds exhibited monomeric emission in chloroform with excited-state lifetimes in the nanosecond timescale. The photoluminescence of the thin solid film of **5b-g** presented clear hypsochromic shifts in the absorbance and emission wavelengths, probably related to H-aggregate formation. Charge transfer between quinoxalines and C_{60} in toluene solution was verified. Overall, the results reported herein show that it is possible to prepare π-conjugate systems based on quinoxaline via the Sonogashira reaction to generate new LLCs, with the potential for application in optoelectronic devices.

Experimental

Materials

All reagents were obtained from commercial sources and used without further purification. Sonogashira couplings were accomplished under nitrogen atmosphere. The terminal acetylenes 1-methyloxy-4-ethynylbenzene (**4a**), 1-hexyloxy-4-ethynylbenzene (**4b**), 1-octyloxy-4-ethynylbenzene (**4c**), 1-decyloxy-4-ethynylbenzene (**4d**), 1-dodecyloxy-4-ethynylbenzene (**4e**), 1-tetradecyloxy-4-ethynylbenzene (**4f**) and 2-(dodecyloxy)-6-ethynylnaphthalene (**4g**) were prepared according to published procedures.[34] The organic solvents were of commercial grade quality, with the exception of THF (HPLC grade), and all were purified by traditional methods. In general, the compounds were purified by column chromatography on silica gel (60–120 mesh) and crystallization from analytical grade solvents. Thin layer chromatography (TLC) was performed Macherey-Nagel, 25 mm a thickness and 5-40 µm particle diameters. For the visualization TLC plates were either placed under ultraviolet light or stained with iodine vapor and acidic vanillin.

Synthesis

3,6-Dibromobenzene-1,2-diamine (2)

In a 250 mL flask were added 4,7-dibromo-2,1,3-benzothiadiazole (2.0 g, 6.8 mmol), THF (15 mL) and ethanol (25 mL). The solution was cooled down using an ice bath and $NaBH_4$ (0.76 g, 34 mmol) was added in small portions under stirring. Finally, cobalt (II) chloride hexahydrate ($CoCl_2.6H_2O$) was added in catalytic amount (1 mol %), making the reaction medium dark and releasing gas H_2S. The mixture was stirred overnight at room temperature and then, filtered to separate the black solid. The solvent was evaporated, water (50 mL) was added and the product was extracted with dichloromethane (3×40 mL). The organic phase was dried over $MgSO_4$ and the solvent removed, resulting in a white solid. **Yield:** 1.80 g (96%). **m.p.:** 87.6 – 90 ℃. **IR (ATR)**: 3397, 3367, 3327, 2962, 1649, 1446, 1259, 1240, 1131, 1065, 1015, 868, 791, 765 cm^{-1}. **^{1}H NMR (400 MHz, $CDCl_3$) δ ppm:** 6,84 (s, 2H); 3,90 (s, broad, 4H).

5,8-Dibromoquinoxaline (3)

In a 100 mL flask was added 3,6-dibromo-1,2-benzenediamine (1.0 g, 3.76 mmol), 30 mL of absolute ethanol, 4 mL of glyoxal solution (40%) and 5 drops of triethylamine. The reaction was stirring at room temperature and light shelter for 12 hours. The precipitate obtained was filtered and recrystallized from ethanol to give a yellow solid. **Yield:** 0.63 g (58%). **IR (ATR):** 3072; 3052; 1873; 1759; 1676; 1584;1451; 1373; 1024; 879; 821. **^{1}H NMR (400 MHz, $CDCl_3$) δ ppm:** 9,01 (s, 2H); 7,99 (s, 2H). **^{13}C NMR (400 MHz, $CDCl_3$) δ ppm:** 146,19; 141,76; 133,89; 124,16.

Preparation of Quinoxaline-based derivatives (5a-g)

A mixture of 5,8-dibromoquinoxaline (**3**) (287 mg, 1.0 mmol), $Pd(PPh_3)_2Cl_2$ (70 mg, 0.1 mmol), CuI (9.5 mg, 0.05 mmol) and PPh_3 (26 mg, 0.1 mmol) in triethylamine/tetrahydrofuran 1:1 (20 mL) was stirred and heating until 70ºC. Then, the respective terminal arylacetylene (**4a–g**) (2.5 mmol) dissolved in tetrahydrofuran (10mL) was added drop wise. The reaction mixture was stirred under reflux for 20min under a nitrogen atmosphere. Cooled down to room temperature, the solution was evaporated, and the crude product was purified by a silica gel chromatography column using hexane/dichloromethane (70:30) as the eluent to afford the respective final compound **5a-g.**

5,8-Bis[(4-methoxyphenyl)ethynyl]quinoxaline: Compound 5a

Yield: 74 mg (55%). **IR (KBr):** 2956, 2919, 2850, 2210, 1602, 1565, 1507, 1464, 1248, 826 cm^{-1}. **^{1}H NMR (400 MHz, $CDCl_3$) δ ppm:** 9.00 (s, 2 H), 7.97 (s, 2 H), 7.64 (d, *J* = 8.0 Hz, Ar-H, 4 H), 6.93 (d, *J* = 8.0 Hz, Ar-H, 4 H), 3.85 (s, -OC*H*$_3$, 6 H). **^{13}C NMR (100 MHz, $CDCl_3$) δ ppm:** 160.1, 145.4, 143.1, 133.6, 133.4, 123.9, 115.0, 114.0, 97.8, 85.1, 55.3. **APPI-MS *m/z:*** Molecular formula $C_{26}H_{18}N_2O_2$ requires $[M+H]^+$ 391.1441; found: 391.1443.

5,8-Bis{[4-(hexyloxy)phenyl]ethynyl}quinoxaline: Compound 5b

Yield: 130 mg (71%). **IR (KBr):** 2954, 2928, 2859, 2206, 1604, 1566, 1509, 1469, 1242, 832 cm^{-1}. **^{1}H NMR (400 MHz, $CDCl_3$) δ ppm:** 9.00 (s, 2 H), 7.96 (s, 2 H), 7.62 (d, *J* = 8.0 Hz, Ar-H, 4 H), 6.92 (d, *J* = 8.0 Hz, Ar-H, 4 H), 4.01 (t, *J* = 6.5 Hz, -OC*H*$_2$, 4 H), 1.80 (m, -OCH_2CH_2, 4 H), 1.47 (m, -$OCH_2CH_2CH_2$, 4 H), 1.36 (m, -CH_2, 8 H), 0.92 (t, -C*H*$_3$, *J* = 6.8 Hz, 6 H). **^{13}C NMR (100 MHz, $CDCl_3$)**

δ ppm: 159.7, 145.4, 143.1, 133.5, 133.4, 123.9, 114.7, 114.5, 98,0, 85.0, 68.1, 31.6, 29.2, 25.7, 22.6, 14.0. **APPI-MS *m/z:*** Molecular formula $C_{36}H_{38}N_2O_2$ requires $[M+H]^+$ 531.3006; found: 530.3008.

5,8-Bis{[4-(octyloxy)phenyl]ethynyl}quinoxaline: Compound 5c

Yield: 157 mg (77 %). **IR (KBr):** 2923, 2853, 2208, 1601, 1563, 1509, 1467, 1243, 829 cm^{-1}. **^{1}H NMR (400 MHz, $CDCl_3$) δ ppm:** 8.99 (s, 2 H), 7.96 (s, 2 H), 7.62 (d, *J* = 8.8 Hz, Ar-H, 4 H), 6.91 (d, *J* = 8.8 Hz, Ar-H, 4 H), 3.98 (t, -OC*H*$_2$, *J* = 6.6 Hz, 4 H), 1.80 (m, -OCH_2CH_2, 4 H), 1.25 (m, -C*H*$_2$, 20 H), 0.89 (t, -C*H*$_3$, *J* = 6.8 Hz, 6 H). **^{13}C NMR (100 MHz, $CDCl_3$) δ ppm:** 159.7, 145.4, 143.1, 133.6, 133.4, 124.0, 114.7, 114.5, 98.0, 85.0, 68.1, 31.8, 29.7, 29.4, 29.2, 26.0, 22.7, 14.1. **APPI-MS *m/z:*** Molecular formula $C_{40}H_{46}N_2O_2$ requires $[M+H]^+$ 587.3632; found: 587.3633.

5,8-Bis{[4-(decyloxy)phenyl]ethynyl}quinoxaline: Compound 5d

Yield: 183 mg (82%). **IR (KBr):** 2954, 2919, 2851, 2203, 1604, 1568, 1509, 1472, 1244, 835 cm^{-1}. **^{1}H NMR (400 MHz, $CDCl_3$) δ ppm:** 9.00 (s, 2 H), 7.97 (s, 2 H), 7.61 (d, *J* = 8.8 Hz, 4 H), 6.91 (d, *J* = 8.8 Hz, 4 H), 4.00 (t, -OC*H*$_2$, *J* = 6.6 Hz, 4 H), 1.83 (m, -OCH_2CH_2, 4 H), 1.48 (m, -$OCH_2CH_2CH_2$, 4 H), 1.33 (m, -CH_2, 24 H), 0.89 (t, -C*H*$_3$, *J* = 6.8 Hz, 6 H). **^{13}C NMR (100 MHz, $CDCl_3$) δ ppm:** 159.7, 145.4, 143.1, 133.5, 133.4, 124.0, 114.7, 114.5, 98.0, 85.0, 68.1, 31.9, 29.6, 29.6, 29.4, 29.3, 29.2, 26.0, 22.7, 14.1. **APPI-MS *m/z:*** Molecular formula $C_{44}H_{54}N_2O_2$ requires $[M+H]^+$ 643.4258; found: 643.4256.

5,8-Bis{[4-(dodecyloxy)phenyl]ethynyl}quinoxaline: Compound 5e

Yield: 199 mg (82%). **IR (KBr):** 2955, 2918, 2851, 2213, 1603, 1567, 1509, 1464, 1245, 829 cm^{-1}. **^{1}H NMR (400 MHz, $CDCl_3$) δ ppm:** 9.00 (s, 2 H), 7.97 (s, 2 H), 7.61 (d, *J* = 8.0 Hz, 4 H), 6.90 (d, *J* = 8.0 Hz, 4 H), 3.99 (t, -OC*H*$_2$, *J* = 6.6

Hz, 4 H), 1.83 (m, -OCH_2CH_2, 4 H), 1.49 (m, -$OCH_2CH_2CH_2$, 4 H), 1.27 (m, -CH_2, 32 H), 0.89 (t, -CH_3, J = 6.8 Hz, 6 H). **^{13}C NMR (100 MHz, $CDCl_3$) δ ppm:** 159.7, 145.4, 143.1, 133.6, 133.4, 123.9, 114.7, 114.5, 98.1, 85.5, 68.1, 31.9, 29.7, 29.6, 29.6, 29.6, 29.4, 29.4, 29.2, 26.0, 22.7, 14.1. **APPI-MS *m/z:*** Molecular formula $C_{48}H_{62}N_2O_2$ requires $[M+H]^+$ 699.4884; found: 699.4879.

5,8-Bis{[4-(tetradecyloxy)phenyl]ethynyl}quinoxaline: Compound 5f

Yield: 190 mg (73%). **IR (KBr):** 2917, 2850, 2362, 1605, 1510, 1471, 1247, 835 cm^{-1}. **^{1}H NMR (400 MHz, $CDCl_3$) δ ppm:** 8.99 (s, 2 H), 7.96 (s, 2 H), 7.61 (d, J = 8.0 Hz, 4 H), 6.90 (d, J = 8.0 Hz, 4 H), 3.98 (t, -OCH_2, 4 H), 1.83 (m, -OCH_2CH_2, 4 H), 1.47 (m, -$OCH_2CH_2CH_2$, 4 H), 1.26 (m, -CH_2, 40 H), 0.88 (t, -CH_3, J = 6.8 Hz, 6 H). **^{13}C NMR (100 MHz, $CDCl_3$) δ ppm:** 159.7, 145.4, 143.1, 133.6, 133.4, 124,0, 114.7, 114.5, 98.0, 85.0, 68.1, 31.9, 29.7, 29.7, 29.6, 29.6, 29.5, 29.5, 29.4, 29.4, 29.2, 26.0, 22.7, 14.1. **APPI-MS *m/z:*** Molecular formula $C_{52}H_{70}N_2O_2$ requires $[M+H]^+$ 755.5510; found: 755.5509.

5,8-Bis{[6-(dodecyloxy)naphthalen-2-yl]ethynyl}quinoxaline: Compound 5g

Yield: 233 mg (84%). **IR (KBr):** 2918, 2851, 2361, 2342, 1625, 1599, 1498, 1467, 1257, 858 cm^{-1}. **^{1}H NMR (400 MHz, $CDCl_3$) δ ppm:** 9.04 (s, 2 H), 8.15 (s, 2 H), 8.04 (s, 2 H), 7.76 – 7,68 (m, 6 H), 7.18 (dd, J = 8.8 and 2.4 Hz, 2 H), 7.13 (d, J = 2.4 Hz, 2 H), 4.09 (t, -OCH_2, J = 6.6 Hz, 4 H), 1.89 (m, -OCH_2CH_2, 4 H), 1.54 (m, -$OCH_2CH_2CH_2$, 4 H), 1.27 (m, -CH_2, 32 H), 0.88 (t, -CH_3, J = 6.8 Hz, 6 H). **^{13}C NMR (100 MHz, $CDCl_3$) δ ppm:** 158.1, 145.5, 143.3, 134.6, 133.6, 132.0, 129.5, 129.1, 128.4, 126.8, 124.1, 119.8, 117.6, 106.6, 98.6, 85.9, 68.2, 31.9, 29,7, 29.6, 29.6, 29.6, 29.4, 29.3, 29.2, 26.1, 22.7, 14.1. **APPI-MS *m/z:*** Molecular formula $C_{56}H_{66}N_2O_2$ requires $[M+H]^+$ 799.5197; found: 799.5199.

Acknowledgments

This study was financed in part by the Coordenação de Aperfeiçoamento de Pessoal de Nível Superior - Brasil (CAPES) - Finance Code 001. The authors acknowledge the following institutions for financial support: CNPq (MCTI/CNPq Nº 422750/2018-2-Universal), INCT/INEO, FAPEMIG, FAPESB (PIBIC) and and PROPP/UFOP grant (#23109.003517/2018-85). The authors are also grateful to CEBIME-UFSC for the HRMS analysis. The authors acknowledge Prof. Hugo Gallardo for fruitful discussions and equipment facilities.

References

[1] Takaoka Y, Ojida A, Hamachi I. Protein Organic Chemistry and Applications for Labeling and Engineering in Live-Cell Systems. Angewandte Chemie International Edition. 2013;52(15):4088-106.

[2] Yang Z, Mao Z, Xie Z, Zhang Y, Liu S, Zhao J, et al. Recent advances in organic thermally activated delayed fluorescence materials. Chemical Society Reviews. 2017;46(3):915-1016.

[3] Hou X, Ke C, Bruns CJ, McGonigal PR, Pettman RB, Stoddart JF. Tunable solid-state fluorescent materials for supramolecular encryption. Nature Communications. 2015;6:6884.

[4] Forrest SR, Thompson ME. Introduction: Organic Electronics and Optoelectronics. Chemical Reviews. 2007;107(4):923-5.

[5] Torsi L, Magliulo M, Manoli K, Palazzo G. Organic field-effect transistor sensors: a tutorial review. Chemical Society Reviews. 2013;42(22):8612-28.

[6] Thejo Kalyani N, Dhoble SJ. Organic light emitting diodes: Energy saving lighting technology—A review. Renewable and Sustainable Energy Reviews. 2012;16(5):2696-723.

[7] Loving GS, Sainlos M, Imperiali B. Monitoring protein interactions and dynamics with solvatochromic fluorophores. Trends in Biotechnology. 2010;28(2):73-83.

[8] Zhang Z, Zheng Y, Sun Z, Dai Z, Tang Z, Ma J, et al. Direct Olefination of Fluorinated Quinoxalines via Cross- Dehydrogenative Coupling Reactions: A

New Near-Infrared Probe for Mitochondria. Advanced Synthesis & Catalysis. 2017;359(13):2259-68.

[9] Carter KP, Young AM, Palmer AE. Fluorescent Sensors for Measuring Metal Ions in Living Systems. Chemical Reviews. 2014;114(8):4564-601.

[10] Aldred MP, Eastwood AJ, Kelly SM, Vlachos P, Contoret AEA, Farrar SR, et al. Light-Emitting Fluorene Photoreactive Liquid Crystals for Organic Electroluminescence. Chemistry of Materials. 2004;16(24):4928-36.

[11] Sagara Y, Yamane S, Mutai T, Araki K, Kato T. A Stimuli-Responsive, Photoluminescent, Anthracene-Based Liquid Crystal: Emission Color Determined by Thermal and Mechanical Processes. Advanced Functional Materials. 2009;19(12):1869-75.

[12] Simpson JCE. Preparation of Quinoxalines from Primary Aromatic O-Diamines and 1,2-Dicarbonyl Compounds. Chemistry of Heterocyclic Compounds. New York: John Wiley and Sons; 1953.

[13] Achelle S, Baudequin C, Plé N. Luminescent materials incorporating pyrazine or quinoxaline moieties. Dyes and Pigments. 2013;98(3):575-600.

[14] Rajule R, Bryant VC, Lopez H, Luo X, Natarajan A. Perturbing pro-survival proteins using quinoxaline derivatives: A structure–activity relationship study. Bioorganic & Medicinal Chemistry. 2012;20(7):2227-34.

[15] Parhi AK, Zhang Y, Saionz KW, Pradhan P, Kaul M, Trivedi K, et al. Antibacterial activity of quinoxalines, quinazolines, and 1,5-naphthyridines. Bioorganic & Medicinal Chemistry Letters. 2013;23(17):4968-74.

[16] Jaung J-Y. Synthesis and halochromism of new quinoxaline fluorescent dyes. Dyes and Pigments. 2006;71(3):245-50.

[17] Gao Z, Qu B, Wu H, Gao C, Yang H, Zhang L, et al. Donor copolymer with benzo[1,2-b:4,5-b′]dithiophene and quinoxaline derivative segments for photovoltaic applications. Journal of Applied Polymer Science. 2014;131(10).

[18] Gao Z, Qu B, Wu H, Yang H, Gao C, Zhang L, et al. A fluorine-functionalized alternating polymer with benzo[1,2-b:4,5-b′]dithiophene and quinoxaline segments for photovoltaic devices. Synthetic Metals. 2013;172:69-75.

[19] Frizon TEA, Duarte RC, Westrup JL, Perez JM, Menosso G, Duarte LGTA, et al. Synthesis, electrochemical, thermal and photophysical characterization of

quinoxaline-based π-extended electroluminescent heterocycles. Dyes and Pigments. 2018;157:218-29.

[20] Liu Z, Liu D, Chen W, Wang J, Li F, Wang D, et al. Asymmetric 2D benzodithiophene and quinoxaline copolymer for photovoltaic applications. Journal of Materials Chemistry C. 2017;5(27):6798-804.

[21] Justin Thomas KR, Lin JT, Tao Y-T, Chuen C-H. Quinoxalines Incorporating Triarylamines: Potential Electroluminescent Materials with Tunable Emission Characteristics. Chemistry of Materials. 2002;14(6):2796-802.

[22] Justin Thomas KR, Velusamy M, Lin JT, Chuen C-H, Tao Y-T. Chromophore-Labeled Quinoxaline Derivatives as Efficient Electroluminescent Materials. Chemistry of Materials. 2005;17(7):1860-6.

[23] Xu X, Yu G, Chen S, Di Ca, Liu Y. Synthesis and characterization of a quinoxaline compound containing polyphenylphenyl and strong electron-accepting groups, and its multiple applications in electroluminescent devices. Journal of Materials Chemistry. 2008;18(3):299-305.

[24] Woody KB, Henry EM, Jagtap S, Collard DM. Synthesis and Characterization of Poly(5,8-quinoxaline ethynylene)s. Macromolecules. 2011;44(23):9118-24.

[25] Kothavale S, Lee KH, Lee JY. Isomeric Quinoxalinedicarbonitrile as Color-Managing Acceptors of Thermally Activated Delayed Fluorescent Emitters. ACS Applied Materials & Interfaces. 2019;11(19):17583-91.

[26] Kulkarni AP, Zhu Y, Jenekhe SA. Quinoxaline-Containing Polyfluorenes: Synthesis, Photophysics, and Stable Blue Electroluminescence. Macromolecules. 2005;38(5):1553-63.

[27] Pina J, de Melo JS, Breusov D, Scherf U. Donor–acceptor–donor thienyl/bithienyl-benzothiadiazole/quinoxaline model oligomers: experimental and theoretical studies. Physical Chemistry Chemical Physics. 2013;15(36):15204-13.

[28] Chen S, Lee KC, Zhang Z-G, Kim DS, Li Y, Yang C. An Indacenodithiophene–Quinoxaline Polymer Prepared by Direct Arylation Polymerization for Organic Photovoltaics. Macromolecules. 2016;49(2):527-36.

[29] Mancilha FS, DaSilveira Neto BA, Lopes AS, Moreira Jr. PF, Quina FH, Gonçalves RS, et al. Are Molecular 5,8-π-Extended Quinoxaline Derivatives

Good Chromophores for Photoluminescence Applications? European Journal of Organic Chemistry. 2006;2006(21):4924-33.

[30] Regis E, Aguiar LdO, Tuzimoto P, Girotto E, Frizon TE, Dal Bó AG, et al. Effect of heteroatom exchange (S/Se) in the mesomorphism and physical properties of benzochalcogenodiazole-based liquid crystals. Dyes and Pigments. 2018;157:109-16.

[31] Dierking I. The Fluid Smectic Phases. Textures of Liquid Crystals: Wiley-VCH Verlag GmbH & Co. KGaA; 2004. p. 91-122.

[32] Demus DG, J. W.; Gray, G. W.; Spiess, H. W.; Vill, L. Handbook of Liquid Crystals, Fundamentals1998.

[33] Rao DSS, Kumar MV, Prasad SK, Hiremath US, Sarvamangala M, Basavaraja S. Novel columnar–calamitic phase sequences in a binary system of bent-core and rod-like mesogens. Journal of Materials Chemistry C. 2013;1(45):7488-97.

[34] Cristiano R, Vieira AA, Ely F, Gallardo H. Synthesis and characterization of luminescent hockey stick-shaped liquid crystalline compounds. Liquid Crystals. 2006;33(4):381-90.

[35] Aguiar LdO, Regis E, Tuzimoto P, Girotto E, Bechtold IH, Gallardo H, et al. Investigation of thermal and luminescent properties in 4,7-diphenylethynyl-2,1,3-benzothiadiazole systems. Liquid Crystals. 2018;45(1):49-58.

[36] Ghosh S, Das S, Kumar NR, Agrawal AR, Zade SS. Effect of heteroatom (S/Se) juggling in donor-acceptor-donor (D-A-D) fused systems: synthesis and electrochemical polymerization. New Journal of Chemistry. 2017;41(20):11568-75.

[37] Valeur B, Berberan-Santos MN. Characteristics of Fluorescence Emission. Molecular Fluorescence: Wiley-VCH Verlag GmbH & Co. KGaA; 2012. p. 53-74.

[38] Yamaguchi Y, Matsubara Y, Ochi T, Wakamiya T, Yoshida Z-i. How the π Conjugation Length Affects the Fluorescence Emission Efficiency. Journal of the American Chemical Society. 2008;130(42):13867-9.

[39] Kato S-i, Yamada Y, Hiyoshi H, Umezu K, Nakamura Y. Series of Carbazole–Pyrimidine Conjugates: Syntheses and Electronic, Photophysical, and Electrochemical Properties. The Journal of Organic Chemistry. 2015;80(18):9076-90.

[40] Reddy TS, Hwang J, Choi MS. Aggregation induced emission properties of naphthalimide–coumarin conjugates with various intermolecular linkages. Dyes and Pigments. 2018;158:412-9.

[41] Coombs BA, Lindner BD, Edkins RM, Rominger F, Beeby A, Bunz UHF. Photophysical property trends for a homologous series of bis-ethynyl-substituted benzochalcogendiazoles. New Journal of Chemistry. 2012;36(3):550-3.

[42] Bayda M, Dumoulin F, Hug GL, Koput J, Gorniak R, Wojcik A. Fluorescent H-aggregates of an asymmetrically substituted mono-amino Zn(ii) phthalocyanine. Dalton Transactions. 2017;46(6):1914-26.

[43] McRae EG, Kasha M. Enhancement of Phosphorescence Ability upon Aggregation of Dye Molecules. The Journal of Chemical Physics. 1958;28(4):721-2.

[44] Kasha M, Rawls HR, Ashraf El-Bayoumi M. The exciton model in molecular spectroscopy. Pure and Applied Chemistry1965. p. 371.

[45] Lakowicz JR. Principles of fluorescence spectroscopy2006.

[46] Noboru M, Yozo K, Masao K. Solvent Effects upon Fluorescence Spectra and the Dipolemoments of Excited Molecules. Bulletin of the Chemical Society of Japan. 1956;29(4):465-70.

[47] Hu J, Xiao Y, Chang Q, Gao H, Cheng X. Effect of the linkages on the self-assembly and photophysical properties of 4,7-diphenyl-2,1,3-benzothiadiazole-based luminescent polycatenars. Journal of Molecular Liquids. 2019;286:110844.

[48] Zeng S, Yin L, Jiang X, Li Y, Li K. D–A–D low band gap molecule containing triphenylamine and benzoxadiazole/benzothiadiazole units: Synthesis and photophysical properties. Dyes and Pigments. 2012;95(2):229-35.

[49] Zhang T, Han H, Zou Y, Lee Y-C, Oshima H, Wong K-T, et al. Impact of Thermal Annealing on Organic Photovoltaic Cells Using Regioisomeric Donor–Acceptor–Acceptor Molecules. ACS Applied Materials & Interfaces. 2017;9(30):25418-25.

Molecular 5,8-π-Extended Quinoxaline Derivatives as Chromophores for Photoluminescence Applications

Leonardo de O. Aguiar[a], Adalberto S. L. Junior[a], Ivan H. Bechtold[b], Sergio Fernando Curcio[c], Thiago Cazati[c], Tiago V. Alves[a] and André Alexandre Vieira[a]

Highlights

- A novel series of fluorescent liquid crystals based on the quinoxaline heterocycle.
- Quinoxalines could form calamitic mesomorphism with nematic and smectic phases.
- Molecules exhibited strong green/yellow photoluminescence in solution and solid.
- Doping of the quinoxalines with fullerene C_{60} suggested charge transfer.